The turbulent fragmentation of the interstellar medium: The impact of metallicity on global star formation.

S. Walch[1]

stefanie.walch@astro.cf.ac.uk

R. Wünsch[2]

richard@wunsch.cz

A. Burkert[3]

S. Glover[4]

and

A. Whitworth[1]

ABSTRACT

We study the influence of gas metallicity, turbulence, and non-equilibrium chemistry on the evolution of the two-phase interstellar medium (warm and cold atomic phases), and thereby constrain the initial conditions for star formation prevailing in turbulent gas. We perform high-resolution simulations in three dimensions, including a realistic non-equilibrium treatment of the ionization state of the gas, and examine both driven and decaying turbulence. This allows us to explore variations in the metallicity Z. In this paper, we study solar metallicity, $Z = Z_\odot$, and low metallicity, $Z = 10^{-3} Z_\odot$, gas. For driven, large-scale turbulence, we find that the influence of the metallicity on the amount of mass in the cold gas component is small. However, in decaying turbulent conditions this picture is much changed. While cold regions survive in the case of solar metallicity, they are quickly heated and dispersed in low-metallicity gas. This result suggests that star formation can be suppressed in environments of low metallicity, unless a strong turbulent driver is acting on time scales shorter than a few turbulent crossing times. Inter alia this finding could explain the overall inefficient star formation as well as the burst-like mode of star formation found in metal-poor, gas-rich systems like dwarf galaxies.

Subject headings: galaxies: high-redshift – galaxies: ISM – galaxies: star formation - ISM: clouds – ISM: evolution – ISM: general

[1]School of Physics and Astronomy, Cardiff University, Queens Buildings, 5 The Parade, CF24 3AA, Cardiff, UK

[2]Astronomical Institute, Academy of Sciences of the Czech Republic, Bocni II 1401, 141 31 Prague, Czech Republic

[3]Universitäts-Sternwarte München, Department für Physik, LMU München, Scheinerstr. 1, 81679 Munich, Ger-

many

[4]Zentrum für Astronomie der Universität Heidelberg, Institut für Theoretische Astrophysik, Albert-Ueberle-Str. 2, 69120 Heidelberg, Germany

1

1. Introduction

The cold interstellar medium (ISM) and, in particular, the molecular part of it, forms the reservoir available for star formation (Wong & Blitz 2002; Kennicutt et al. 2007; Bigiel et al. 2008). The properties of this cold gas component regulate the mass distribution of prestellar cores in a molecular cloud (e.g., Padoan & Nordlund 2002, 2011; Hennebelle & Chabrier 2008; Heitsch et al. 2008), and hence the stellar initial mass function (IMF; e.g., Motte et al. 1998; Nutter & Ward-Thompson 2007). It has been suggested that star formation within a molecular cloud is regulated by the interplay of gravity and turbulence (e.g., Klessen et al. 2000). However, on galactic scales, understanding the formation and the properties of the cold gas reservoir available for star formation is equally important. In addition to turbulence and gravitational collapse, heating and cooling processes essentially determine the distribution of the cold ISM and therefore the global star formation efficiency (Ostriker et al. 2010).

The ISM is highly turbulent, with gas velocity dispersions of up to 50 times the sound speed of the molecular (10 K) gas component in local galaxies, and even higher factors in high-redshift disk galaxies (Genzel et al. 2006). However, turbulence has been shown to dissipate quickly (Mac Low 1999) if the external driving is stopped, resulting in the need to continuously drive turbulence either *locally* via stellar feedback (Ostriker et al. 2010) or *globally* via, e.g., galaxy mergers (Teyssier et al. 2010; Karl et al. 2010), clumpy infall of cold gas (Elmegreen & Burkert 2010; Aumer et al. 2010), or spiral density waves.

At the same time, the ISM is regulated by metallicity-dependent heating and cooling processes that tend to segregate it into distinct, thermally stable phases (warm and cold), which can coexist in approximate pressure equilibrium. The transition between the phases is driven by thermal instability (TI; Field 1965; Burkert & Lin 2000), more specifically by its isobaric mode (e.g., Pikel'Ner 1968; McKee & Ostriker 1977; Wolfire et al. 1995). Thus, for several reasons the efficiency with which a galaxy is able to form cold gas depends on the metal content of the gas. First, the turbulent shock compression of the ISM depends on the metallicity-dependent cooling rate

(e.g., Omukai et al. 2005). Second, within the cold component, the dust abundance (i.e., metallicity) controls the conditions under which the transition from cold atomic to molecular gas occurs (Gnedin et al. 2009; Krumholz et al. 2009; Glover & Mac Low 2011). Third, depending on the strength of the interstellar radiation field, low gas metallicities ($\leq 0.01Z_\odot$) alter the balance of heating and cooling in such a way that the development of a bi-stable phase can be suppressed (see semi-analytical estimates by Spaans & Carollo 1997; Spaans & Norman 1997). This conclusion has also been drawn by Schaye (2004) who used equilibrium models and the CLOUDY software to demonstrate that the formation of cold gas is a metallicity dependent process. His models are successfully employed to predict the outer edges of standard star forming galactic disks, for both regular spirals and dwarfs (Leroy et al. 2008).

The idea that the (extra-)galactic star formation efficiencies are connected to the present ISM properties has been further discussed in several recently developed theoretical models (Elmegreen 2002; Krumholz & McKee 2005; Schaye & Dalla Vecchia 2008; Gnedin et al. 2009; Krumholz et al. 2009; Pelupessy & Papadopoulos 2009; Krumholz et al. 2011). Some of them estimate the effects of turbulence and have shown that the thermodynamics of the ISM can control the resulting shape of the density probability density function (PDF) of the ISM gas (Wada & Norman 2007; Tasker & Bryan 2008; Robertson & Kravtsov 2008). The numerical simulations we present here indicate that the density PDF is only strongly affected in the non-driven turbulent case.

Previous highly resolved studies of the statistics of driven or decaying turbulence mostly assumed the gas to be isothermal (e.g., Kritsuk et al. 2007; Beresnyak & Lazarian 2009, including magnetic fields). First steps toward a detailed numerical model of turbulence including gas thermodynamics have been published by Kritsuk & Norman (2004), Joung & Mac Low (2006), Brandenburg et al. (2007), and de Avillez & Breitschwerdt (2007), who include parameterized cooling functions at solar metallicity. Kritsuk & Norman (2004) and Brandenburg et al. (2007) study the amount of turbulence generated by the TI itself, whereas Joung & Mac Low (2006) and de Avillez & Breitschwerdt (2007) use supernova ex-

plosions as internal drivers of turbulence. Other authors have studied molecular cloud formation in colliding flows in two dimensions (Audit & Hennebelle 2005; Heitsch et al. 2006, 2008) and three dimensions (Slyz et al. 2005; Vázquez-Semadeni et al. 2007; Hennebelle et al. 2008; Banerjee et al. 2009) using parameterized cooling and heating processes. In these simulations turbulence is generated via various instabilities occurring in the collision layer of the flow. These studies confirm the development of a multi-peaked density and temperature PDF when turbulence and equilibrium-based gas thermodynamics are treated simultaneously. On the other hand, Vazquez-Semadeni (2009) conclude that turbulence acts faster than TI, and thus relegates classic instabilities (Field 1965) to a secondary role in controlling the gas dynamics. He shows that shock-compressed diffuse gas can stay in an unstable regime for a few megayears before cooling efficiently. This is supported by recent models of de Avillez & Breitschwerdt (2010) who point out that the treatment of non-equilibrium ionization is essential for a correct treatment of the highly dynamical ISM evolution, at least in the high temperature regime.

In this paper, we show that the formation and evolution of the cold ISM phase is a highly metallicity dependent process. We base this conclusion on high-resolution, three-dimensional simulations with the Eulerian grid code FLASH (Fryxell et al. 2000), including both driven and decaying turbulence, as well as metallicity-dependent heating and cooling (Glover et al. 2010). We demonstrate the major influence of the gas metallicity in decaying conditions – a finding which highlights the global metallicity dependence of star formation. We suggest that this result may explain puzzling observations, like the low star formation rates in metal-poor, gas-rich galaxies.

2. Numerical Method

We use FLASH 3.2, an MPI parallel Eulerian grid code, which solves the Euler equations for fluid flow. We modify the energy equation to include heating and cooling effects (see Section 2.2). The implemented directionally split, finite difference scheme is based on the piecewise parabolic method (PPM; Woodward & Colella 1984; Colella & Woodward 1984) in its direct Eulerian form.

PPM allows one to model strong shocks and discontinuities with high accuracy. Using the method of characteristics, the nonlinear flux of quantities between zones is obtained by solving a Riemann problem at each zone boundary in alternating one-dimensional sweeps through the grid. We use the hybrid Riemann solver (HLLE) inside shocks to avoid odd-even instabilities (Hussaini et al. 1997).

2.1. Turbulence

At every time step, supersonic turbulence is driven on the largest spatial scales ($1 \leq k \leq 3$, where $k = 1$ corresponds to $2\pi/500\mathrm{pc}$ and $k = 3$ corresponds to $2\pi/166\mathrm{pc}$). The driving energy input rate per unit mass, $dE_{\mathrm{in}}/dt = 1.04 \times 10^{-2}\mathrm{erg\,g^{-1}s^{-1}}$, is chosen such that supersonic turbulence develops, with a roughly constant root-mean-squared (rms) velocity of $50\,\mathrm{km\,s^{-1}}$. We use a mixture of solenoidal and compressive forcing with random phases and time-correlated driving forces, which leads to coherent large-scale structures. The phases of the driving modes are modulated on a turnover timescale, $\tau_{\mathrm{dyn}} = 50$ Myr, which is equal to five turbulent crossing times, or about 70% of a sound crossing time for gas at the initial temperature of 5000 K. For each mode and at each time step six separate phases (real and imaginary in three dimensions) are evolved by an Ornstein-Uhlenbeck random process, which represents a velocity in Fourier space.

2.2. Chemistry and Cooling

Gas dynamics and gas chemistry are strongly coupled and should be solved at the same time (Glover et al. 2010). In order to study the metallicity dependence of the multi-phase ISM, we include a basic and fast chemical network, based on Glover & Mac Low (2007), to follow a limited amount of non-equilibrium gas chemistry, specifically the chemistry involved in the determination of the ionization fraction of the gas. When solving the energy equation we take account of radiative cooling due to line emission (Lyα, C_{II}, O_{I}, and Si_{II}) and dust, and the chemical cooling produced by the collisional ionization and radiative recombination of hydrogen. We account for heating due to cosmic rays, X-rays, and photoelectric emission from small grains and polycyclic aromatic hydrocarbons (PAHs). For the ultraviolet background radiation field, we use the standard estimate of

Draine (1978). In this study, we neglect the effects of dust shielding. This is a reasonable approximation in the warm gas in our solar metallicity simulation, but may cause us to overestimate the temperature of the dense component; a colder dense component would in any case strengthen our conclusions. It is a very good approximation throughout our low-metallicity simulation, as in this case the dust extinction is very small even in the cold clumps. For the cosmic ray ionization rate of neutral hydrogen, we adopt a value $\zeta_H = 3 \times 10^{-17} \mathrm{s}^{-1}$, while for the X-ray ionization and heating rates, we use the values given in Appendix A of Wolfire et al. (1995), assuming a fixed absorbing column of hydrogen $N_H = 10^{20}$ cm^{-2}.

We do not include the formation and destruction of molecular hydrogen (H$_2$) in our current models. This may be a significant coolant in the warm, diffuse ISM in the Galaxy (Gnedin & Kravtsov 2010), although this remains unclear. However, it is very unlikely to be a significant coolant in the warm gas in our low-metallicity simulation, as its equilibrium abundance would be very small, even if gas-phase formation mechanisms were included (Glover 2003). We would therefore expect the inclusion of H$_2$ chemistry and cooling to merely heighten the differences between the results of our solar metallicity and low-metallicity runs.

The heating and cooling terms, and also the chemical source and sink terms, are operator split from the advection and pdV work terms and are solved implicitly using the DVODE solver (Brown et al. 1989). In cases where the chemical or cooling timesteps are much shorter than the hydrodynamic time step, sub-cycling is used to treat the cooling and chemistry, thereby avoiding the need to constrain the global time step. Chemical abundances are represented as tracer fields and are advected using the standard FLASH infrastructure for such fields.

2.3. Initial Conditions and Resolution

Our initial conditions are motivated by typical ISM values. At $t = 0$, we start from a homogeneous box with a total mass of 3.99×10^6 $M_\odot$. The box length is $L = 500$ pc, the initial gas density $\rho_0 = 2.16 \times 10^{-24}$ g cm^{-3}, and the initial temperature is set to 5000 K. Turbulent driving with the energy input rate given in Section 2.1 results in an rms turbulent velocity of 50 km s^{-1}, and so the initial rms Mach number is approximately 7. We show results for two different gas metallicities: solar metallicity (hereafter *Z0*) and low metallicity $Z = 10^{-3} Z_\odot$ (hereafter *Z-3*). We use a 512^3 grid without AMR for all of the runs presented. With this setup each cell has a volume of $(0.977$ pc$)^3$.

3. Results

We first evolve the box by driving turbulence for one turnover time $\tau_{\mathrm{dyn}} = 50$ Myr. Thereafter, driving is switched off, and the gas is evolved for a further turnover time, up to $t = 100$ Myr. In the following sections, we discuss the most striking features and differences of these two evolutionary stages with respect to the gas metallicity.

3.1. Driven turbulence

Starting from a homogeneous gas density distribution, a two-phase medium is quickly generated due to the influence of driven, supersonic turbulence, which produces strong non-linear fluctuations in all thermodynamic variables. Kinetic energy is injected on large scales and cascades to increasingly smaller ones. This turbulence generates shocks that compress the warm, neutral medium into dense, cold filaments.

Regardless of the gas metallicity, regions with very low density ($\rho < 10^{-27}$g cm^{-3}) and very high density ($\rho > 4 \times 10^{-22}$g cm^{-3}) develop quickly, after only 5 Myr $= 0.1$ τ_{dyn}. The metallicity influences the maximum density reached, ρ_{max}, which is about a factor of eight larger in the solar metallicity run compared to the low-metallicity run. However, this is a relatively small difference compared to the total range of densities.

In isothermal compressible turbulence the volume-weighted density PDF is expected to follow a log-normal distribution (Mac Low 1999; Ostriker et al. 2001; Kritsuk et al. 2007; Federrath et al. 2008; Kitsionas et al. 2009) of the form

$$p(s)ds = \frac{1}{\sqrt{2\pi\sigma^2}} \exp\left[-\frac{(s-s_0)^2}{2\sigma^2}\right]ds. \quad (1)$$

where $s = \ln(\rho/\rho_0)$ is the logarithmic density contrast, with ρ_0 equal to the mean gas density. In Equation (1), σ is the logarithmic density dispersion, and s_0 is the mean value of s.
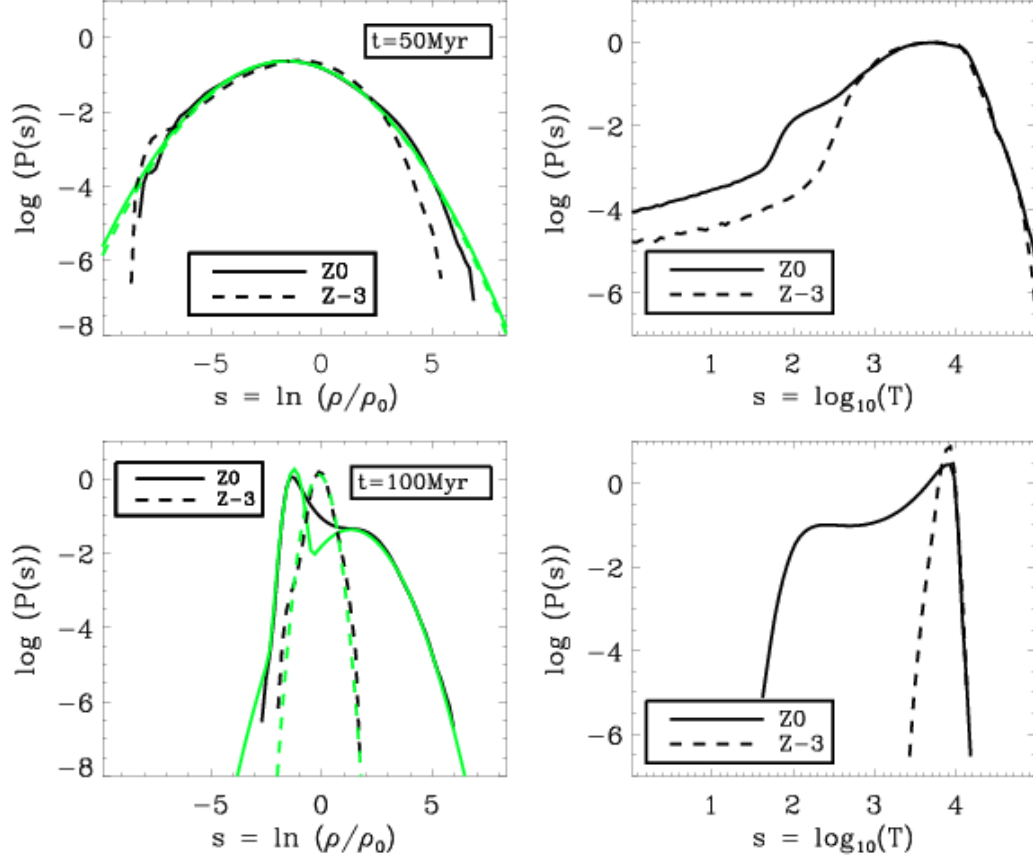
Fig. 1.— Density and temperature PDFs after 1 τ_{dyn} of evolution under driven conditions (upper panels) and after another τ_{dyn} of evolution under decaying conditions (lower panels). Solid black lines: case $Z0$; dashed black lines: case Z-3; green lines: log-normal fits (see Table 1).

In Figure 1 (upper left panel) we show the resulting density PDFs after driving turbulence for a turnover time (i.e., five turbulent crossing times). Where appropriate, we include fits according to Equation (1), and summarize the resulting values for σ and s_0 (or $\rho(s_0) = \rho_0 \exp(s_0)$, respectively) in Table 1. In the driven case, the density PDFs are well described with a single log-normal function for both *Z0* and *Z-3*. For *Z0* the distribution is slightly asymmetric and skewed toward higher densities. However, the best fits result in a similar variance of $\sigma \simeq 1.7$ in both cases. Studies of driven turbulence in isothermal gas have found a relationship between σ and the rms Mach number M (Padoan et al. 1997; Padoan & Nordlund 2002; Price et al. 2011)

$$\sigma^2 = \ln\left(1 + b^2 M^2\right), \qquad (2)$$

where the value of the parameter b depends on the relative importance of the compressive and solenoidal modes (Federrath et al. 2008). For the driving used in our simulations, $b = 0.5$, and the rms Mach number at $t = 50$ Myr is 8.66 in the solar metallicity simulation, and 9.26 in the low-metallicity simulation. Equation (2) therefore predicts that $\sigma = 1.72$ for the solar metallicity simulation and $\sigma = 1.76$ for the low metallicity simulation, in good agreement with our measured value of 1.7.

We emphasize that our finding of a broad, but single-peaked density PDF supports the conclusions of Vazquez-Semadeni (2009), where he argues that supersonic turbulence should dominate the evolutionary state of ISM gas because it acts faster than conventional TIs. We note that a single-peaked density PDF has also been found by de Avillez & Breitschwerdt (2007). However, models by e.g., Slyz et al. (2005), who drive turbulence in colliding flows, result in a double-peaked density PDF. We suggest that the transition between single- and double-peaked density PDF profile depends on the strength of the turbulence, i.e., the Mach number. This suggestion is verified below (Section 3.2).

The temperature PDFs, which are also shown in Figure 1 (upper right panel) cannot be well approximated with a single log-normal distribution, which only gives acceptable fits for the high temperature parts. Toward low temperatures (i.e.,

for $T < 300$K), the distributions show extended powerlaw tails. This behavior is caused by the cooling instability that separates the warm and cold neutral gas.

Overall, we find the temperature distributions to be more strongly affected by the gas metallicity than the density PDFs. In particular, the volume filling factors (VFFs) of the cold components differ significantly. For further analysis, we define *the cold component* to be all gas with $T < 300$K, as 300 K is the temperature threshold below which a stable, cold atomic phase can exist (Wolfire et al. 2003). Then we find 1.7% of the computational domain to be cold for *Z0*, whereas we find only 0.075% to be cold for *Z-3*.

In Figure 2, columns A and B, we show the density (top panels) and temperature (bottom panels) of the evolved filamentary structures in the $z = 0$ plane. Prima facie the density distributions of the solar metallicity (panel (A)) and the low-metallicity case (panel (B)) look similar, in agreement with the PDFs. However, the filamentary structure formed in run *Z-3* seems to be coarser and individual filaments seem to be less condensed than in run *Z0*.

When comparing the two-dimensional density and temperature distributions (Figure 2), we find both shock heating and pdV heating as well as radiative cooling and cooling by expansion to be very important. The presence of shock-heated regions surrounding dense and cool filaments can be found in both the *Z0* and the *Z-3* case. However, most of the cold regions in run *Z-3* can be identified with voids in the density structures (see also Figure 3). Thus, these regions have cooled due to expansion. Radiatively cooled regions within dense filaments are very rare in run *Z-3*, whereas these dominate the cold part in run *Z0*. It should be noted that for *Z0* the mean density in the cold gas is higher than the mean density in the warm gas ($T > 300$K), as expected for gas which truly undergoes a cooling instability. However, for *Z-3* this is not the case (see Table 1). This indicates that cooling due to expansion is dominant in case *Z-3* whereas the dense, cold component is very small. Thus, our results confirm previous semi-analytical estimates (e.g., Schaye 2004) that the
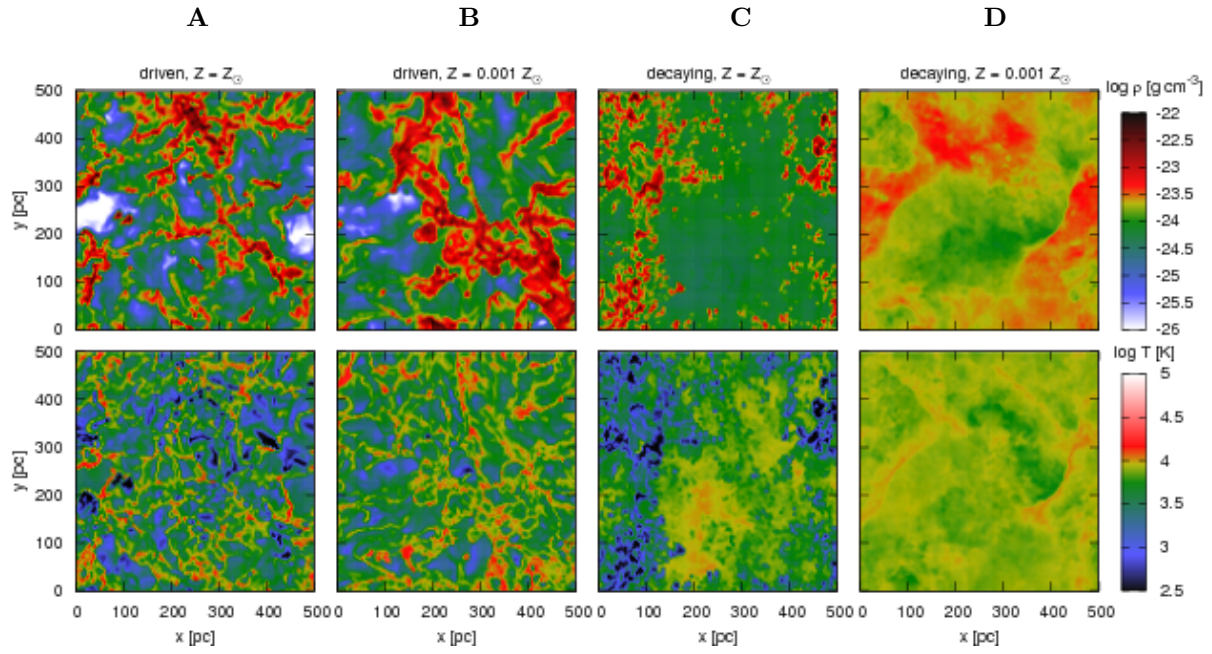
Fig. 2.— Cuts through the computational volume on the $(z = 0)$-plane, showing the density and temperature of the developed two-phase media after supersonic turbulence has been driven for five turbulent crossing times (panels (A) and (B)), and then allowed to decay for a further five turbulent crossing times (panels (C) and (D)). Panel (A) and (C) depict the solar metallicity case, *Z0*, whereas panel (B) and (D) show the low-metallicity case, *Z-3*.

formation of stable molecular cloud cores might be strongly inhibited in low-metallicity gas.

3.2. Decaying turbulence

Starting from the evolved turbulent setup discussed before, we switch off turbulent driving at $\tau_{\rm dyn} = 50$ Myr, and study the evolution of the gas under decaying conditions until $t = 2\,\tau_{\rm dyn}$. In Figure 3 (upper panel) we show the evolution of the rms velocity dispersion, $v_{\rm rms}$, for the full time interval. After driving has been switched off $v_{\rm rms}$ decreases. From initially close to $50{\rm kms}^{-1}$, $v_{\rm rms}$ drops down to $20{\rm kms}^{-1}$ within 5 Myr ($t = 55$ Myr) and to $10{\rm kms}^{-1}$ within approximately 25 Myr ($t = 75$ Myr). In Figure 3 (lower panel) we depict the decay of kinetic energy. We find that both cases, Z0 and Z-3, are well described by the fitting formula derived by Pavlovski et al. (2002)

$$E(t) = E_0(1 + t/t_1)^{\eta}, \qquad (3)$$

where E_0 is the initial kinetic energy and $t_1 = L_{\rm inj}/v_{\rm rms}$ is equal to the initial ratio of mean energy injection scale to the rms velocity. For isothermal, compressible MHD turbulence, Mac Low (1999) derived $\eta \approx -1$. Kitsionas et al. (2009) also extracted $\eta = -1$ for compressible HD turbulence. Incompressible, non-magnetic turbulence has been found to decay somewhat faster with η in $[-1.2, -1.4]$. In addition, cooling has been found to accelerate the decay as the average Mach number is larger (Kritsuk & Norman 2002; Pavlovski et al. 2002). With cooling and MHD turbulence, Pavlovski et al. (2002) derived $\eta \approx -1.3$, whereas Kritsuk & Norman (2002) found indices between -1 and -2. We derive $\eta \approx -1.3$ for Z-3. For Z0 we find a slow decay within the first 10 Myr ($\eta \approx -1$), but a steep decay thereafter with $\eta \approx -1.8$ from 10 Myr ($t = 60$ Myr) onward. Due to the fact that cooling is much more efficient in the case of solar metallicity, Z0 (see Section 4.1 for a discussion of the mass fraction in cold gas), and based on previous findings that the decay is accelerated with cooling, our findings are in overall agreement with the expectation that η should be lower for Z0 than for Z-3.

Returning to Figure 1, we show the temperature and density structure of run Z0 (panel (C))

and run Z-3 (panel (D)) after turbulence has decayed for 50 Myr. In this case we find striking differences between Z0 and Z-3. Whereas cold clumps survive in run Z0, they are completely dispersed in run Z-3. In fact, we find all of the cold gas in Z-3 to be warmer than 300 K after 10 Myr (i.e., at $t = 60$ Myr).

In agreement with this qualitative finding, the metallicity also has a major impact on both density and temperature PDFs (see lower panels in Figure 1). All distributions show a significant decrease in variance as the system evolves toward its equilibrium density and temperature configuration. In run Z-3 a single-peaked density PDF remains. However, now the variance of the distribution is so small that we can speak of a single, warm phase. All of the cold gas has been heated and therefore the VFF of the cold component is 0. In this environment star formation is basically impossible. This is in agreement with the findings of Schaye (2004) and Spaans & Norman (1997), who predict that star formation is strongly suppressed in low-metallicity environments.

For run Z0, the single log-normal density PDF is replaced by a combination of two log-normals representing two distinct gas phases, a warm diffuse and a cold dense phase. A double-peaked density PDF has been previously reported by authors like Slyz et al. (2005) and Audit & Hennebelle (2010), who employed cooling functions. In contrast to their work, the separation into two distinct phases seems to be less clean in our case. We note that the blurring of the warm and cold phases is probably a consequence of our chemodynamical model. We expect the separation to become increasingly clear as the turbulence decays further and $v_{\rm rms}$ decreases. We will discuss the time evolution of the density PDFs for different turbulent driving energies in a subsequent paper. Finally, the VFF or of the cold component is slowly increasing in the case of Z0, and reaches 4% at $t = 100$ Myr.

4. Discussion

In the following, we discuss the impact of turbulence and non-equilibrium chemistry on the dynamical evolution of the ISM.
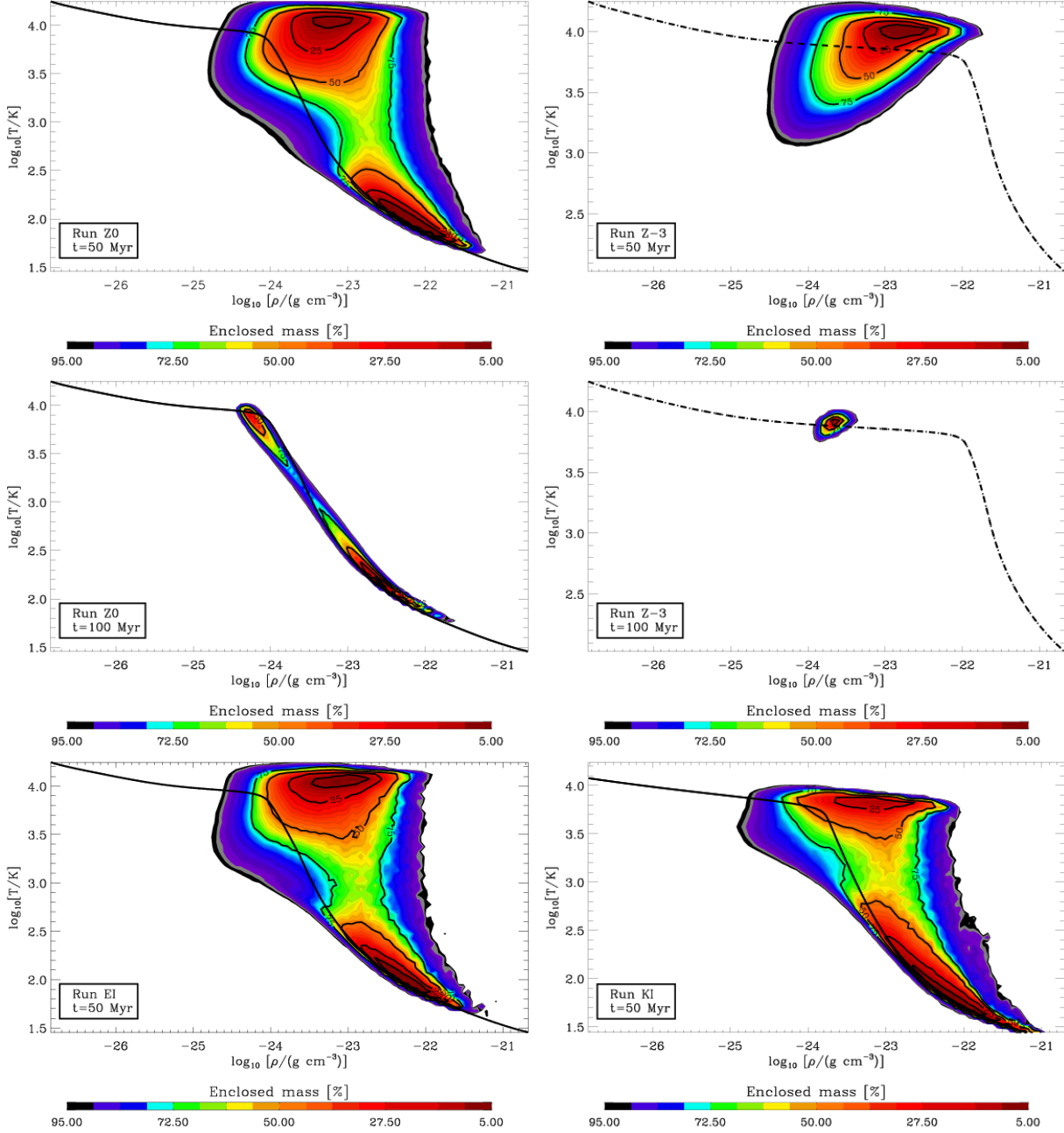
Fig. 4.— Cumulative mass distributions derived for driven turbulence at $t = 50$ Myr (top row; see Figure 2 columns A and B) and for decaying turbulence at $t = 100$ Myr (middle row; see Figure 2 columns C and D). The equilibrium curves of density and temperature for $Z_0 = 1\,Z_\odot$ (black solid line, left column) and $Z_0 = 10^{-3}\,Z_\odot$ (black dashed line, right column) are plotted on top. For comparison we show the mass distributions of runs EI and KI (bottom row), both at the end of the driven period at $t = 50$ Myr. See Section 4.2 for further details on these runs EI and KI.

9

Run	Time [Myr]	Max [g cm^{-3}]	Mean Warm [g cm^{-3}]	Mean Cold [g cm^{-3}]	Fit $\rho(s_0)$	σ
Z0	50	2.4×10^{-21}	1.65×10^{-24}	3.35×10^{-23}	4.4×10^{-25}	1.73
Z-3	50	3.2×10^{-22}	2.07×10^{-24}	7.33×10^{-25}	4.6×10^{-25}	1.70
Z0	100	1.0×10^{-21}	5.83×10^{-25}	1.22×10^{-23}	6.3×10^{-25}	0.22
					8.2×10^{-24}	0.93
Z-3	100	1.2×10^{-23}	9.27×10^{-25}	–	1.9×10^{-24}	0.31

Table 1: Absolute Maximum (Column 3) and Mean Densities (Columns 4 and 5) Extracted from the Simulations. The first two rows are for the part of driven turbulence, the following three rows are for the part of decaying turbulence. The mean densities are time averages over 50 Myr for the warm ($T \geq 300$K, Column 4) and cold ($T < 300$ K, Column 5) gas components individually. For reference, the mean gas density summed over both components was 2.16×10^{-24} g cm^{-3} throughout. We also list the parameters for the log-normal fits to the density PDFs shown in Figure 1. The parameters are described in Equation (1). For run *Z0* we list two sets of parameters at $t = 100$ Myr as this distribution can only be fitted with the sum of two log-normal functions (see Figure 1).

4.1. Metallicity dependence

In Figure 4 (upper and central panels) we show the equilibrium density-temperature curves for low and solar metallicity together with the mass distributions found in *Z0* and *Z-3* at 50 Myr and 100 Myr. At low densities ($\rho \lesssim 10^{-24}$g cm^{-3}) and high temperatures, cooling is dominated by Lyα and therefore the metallicity dependence is negligible. For higher densities and lower temperatures, the cooling rate is dominated by fine structure emission from C$^+$ and O, and is therefore strongly dependent on Z.

Based on comparing the equilibrium curves for low and high Z, it might at first seem surprising that both runs (*Z0* and *Z-3*) look so similar in case of driven turbulence and show a log-normal profile which is single-peaked, just like in an isothermal case. Therefore we conclude that the shape of the density PDF (single or double peaked; see Figure 1) is not only a function of the employed gas thermodynamics but at the same time must be a function of the turbulent Mach number. Strongly driven turbulence (Vazquez-Semadeni 2009) causes the gas to populate a large region of parameter space in the (ρ, T)-plane significantly displaced from the equilibrium locus. As a result, the density PDF in the case of driven turbulence is broad, but single-peaked just like in an isothermal simulation (Figure 1, upper panels). Even at late stages of the evolution ($t = 100$ Myr), where $v_{\rm rms}$ has decayed to 7 kms^{-1}, the separation into two phases is less distinct than in previous models (Slyz et al. 2005; Audit & Hennebelle 2010). A closer investigation reveals that, apart from the different thermodynamics schemes employed, also the Mach number seems to be lower in these models than in our simulations. For instance, Audit & Hennebelle (2010) who reported a clearly double peaked profile had generally low turbulent Mach numbers (the Mach number is around 1 in Audit & Hennebelle 2010). On the other hand, authors who used efficient driving mechanisms (de Avillez & Breitschwerdt 2007) also reported single-peaked distributions despite including gas heating and cooling. We therefore infer that a pronounced double-peaked density PDF is a sign of a two-phase medium at low Mach numbers.

Even though the density PDFs in the driven turbulent cases look similar and seem to be independent of the gas metallicity, we find the respective mass distributions in the (ρ, T)-plane to be quite different. For *Z0*, a large fraction of the gas is in the thermally unstable regime, in agreement with observations (e.g., Kanekar et al. 2003). Moreover, for *Z0*, low temperature values preferentially coincide with high-density values. For *Z-3*, the opposite trend is found. Here, lower temperature values correspond to lower densities. In general, only a small mass fraction is found to
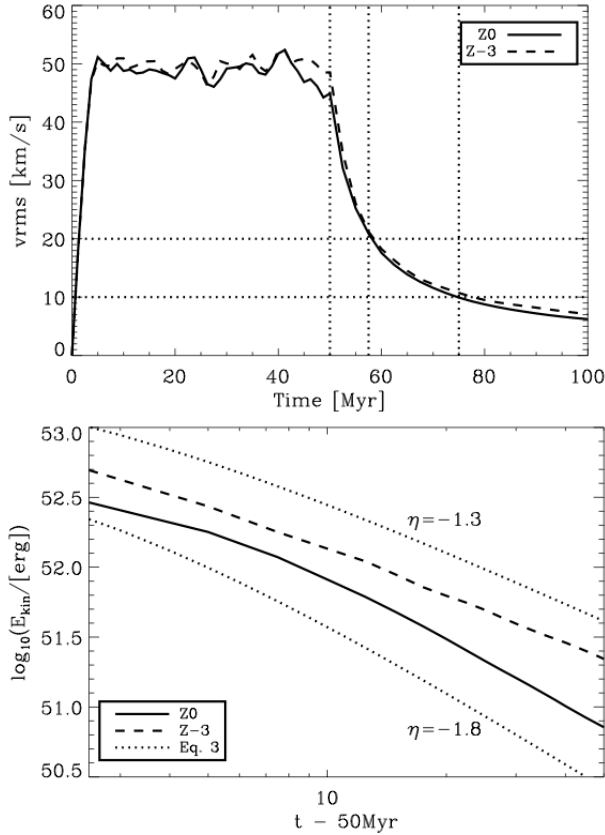
Fig. 3.— Upper panel: we depict the root mean square velocity as a function of time. From left to right, the first dotted vertical line marks the beginning of the decay phase at $t = 50$ Myr, the following two dotted horizontal and vertical lines mark the points at which the turbulence has decayed to $v_{\rm rms} = 20 {\rm kms}^{-1}$ (55 Myr) and $v_{\rm rms} = 10 {\rm kms}^{-1}$ (75 Myr), respectively. Lower panel: decay of kinetic energy for the second 50 Myr of evolution. We show both cases, *Z0* (solid line) and *Z-3* (dashed line), as well as the decay curves derived from Equation (3) (dotted lines) for $\eta = -1.3$ and $\eta = -1.8$. The kinetic energy decay is faster in solar metallicity gas.
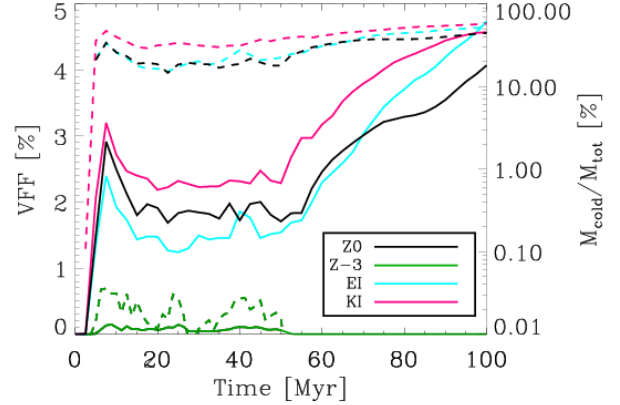
Fig. 5.— Time evolution of the volume filling factor (solid lines) and the mass fraction (dashed lines) of the cold gas ($T < 300$ K). Turbulent driving was switched off at $t = 50$ Myr. We show all four runs: *Z0* (black), *Z-3* (green), *EI* (turquoise), and *KI* (magenta).

be at temperatures less than 1000 K, as cold gas preferentially coincides with regions of low density, where expansion is the main cooling process.

We now determine the fraction and the VFF of the cold gas formed in our simulations. For decreasing metallicity the equilibrium temperature, $T_{\rm equi}$, remains high ($T_{\rm equi} > 300$ K) up to increasingly high density. For further reference, we define the threshold density $\rho_{\rm thres}$ above which gas may cool below 300 K. For $Z_0 = Z_\odot$, we find $\rho_{\rm thres} \simeq 9 \times 10^{-24}$ g cm^{-3}, and for $Z_0 = 10^{-3} Z_\odot$ we find $\rho_{\rm thres} \simeq 5 \times 10^{-22}$ g cm^{-3}. Thus, for $Z_0 = Z_\odot$ some of the gas reaches densities higher than $\rho_{\rm thres}$, whereas for $Z_0 = 10^{-3} Z_\odot$, $\rho_{\rm max}(Z-3) = 3.2 \times 10^{-22}$ g cm^{-3} and $\rho_{\rm thres} > \rho_{\rm max}$ (see Section 3.1 and Table 1).

The strong influence of the gas metallicity on the formation and survival of cold coherent clumps only reveals itself during the non-driven, decaying phase, as the temperature and density PDFs of the two simulations are very similar during the driven turbulent period. After turbulent driving has been switched off (Figure 4, middle panels) the systems evolve toward local equilibrium. Consequently, the almost immediate disappearance of the cold

component in run *Z-3* can be explained. The cold component formed in the driven case was solely a product of turbulent stirring. Regions of high density, cold gas, which truly undergo thermal instability are rare at low metallicity since the high threshold density required for the formation of a stable cold component cannot be reached. Therefore, when evolved under decaying conditions, the cold gas is quickly heated up and no cold and dense clumps remain.

This result is reinforced by the time evolution of the VFF of the cold gas component, and of the mass in cold gas, shown in Figure 5. With driven turbulence the VFF is roughly constant and about 20 times lower in *Z-3* than in *Z0*. With decaying turbulence the two cases diverge as VFF is slowly increasing for *Z0* whereas it quickly approaches 0 for *Z-3*. The mass fraction of gas found in the cold component evolves in a similar manner as the VFF. However, even in the driven case, the mass in cold gas is more than a factor of 1000 lower for *Z-3* than for *Z0* (with an average of 10^3 $M_\odot$ for *Z-3*, corresponding to only 0.025% of the total mass, compared to an average of 10^6 $M_\odot$ for *Z0*, corresponding to a substantial fraction of the total mass, i.e., 25%).

4.2. The impact of non-equilibrium chemistry

In the following, we analyze the impact of non-equilibrium chemistry on our findings. To quantify the degree of any departures from thermal equilibrium in runs *Z0* and *Z-3* we first monitor the mean difference between actual gas temperature and expected equilibrium temperature in Figure 6 (solid and dashed line). In the case of solar metallicity, *Z0*, we find a significant offset, ΔT, of the actual gas temperature from the equilibrium temperature, in agreement with Figure 4 (upper left panel). In the decaying period ($t > 50$Myr) ΔT then decreases, as does the turbulent Mach number. For *Z-3*, the system is close to equilibrium throughout the simulation and ΔT is small.

Two possible causes of the high ΔT in run *Z0* are: (1) non-equilibrium chemical effects and (2) efficient thermalization of turbulent energy on a time scale shorter than the cooling time scale. To investigate the importance of the non-equilibrium chemistry on the gas heating and cooling, we performed two comparison runs at $Z = Z_\odot$ that do

not take into account non-equilibrium effects. In run *EI*, we still consider the detailed Glover et al. cooling function when solving the energy equation, but at the same time we assume chemical equilibrium. In run *KI* we completely neglect the chemical network as well as the detailed cooling function, and instead use the parameterized cooling function:

$$\Gamma = 2.0 \times 10^{-26} \text{erg s}^{-1}, \tag{4}$$
$$\frac{\Lambda(T)}{\Gamma} = 10^7 \exp\left(\frac{-1.184 \times 10^5}{T + 1000}\right)$$
$$+ 1.4 \times 10^{-2} \sqrt{T} \exp\left(\frac{-92}{T}\right) \text{ cm}^3, \tag{5}$$

which is based on Koyama & Inutsuka (2000, 2002) (see also Vázquez-Semadeni et al. 2007).

We include the results for both *EI* and *KI* in Figures 4 (bottom row), 5, and 6. From Figure 4, we find that the phase space mass distribution formed in run *EI* is almost identical to run *Z0*. Thus, non-equilibrium chemistry seems to have a minor effect at high driving velocities. We conclude that the offset of the mass distribution with respect to the equilibrium curve as well as the high ΔT in Figure 6 are caused by turbulent shock compression and extra heating associated with turbulent dissipation. Run *KI* supports this picture, although we find *KI* to differ from *EI* and *Z0* in mass distribution (see Fig. 4, bottom right panel) and mean temperature (see Figure 6). Overall, run *KI* is closer to thermodynamical equilibrium throughout the whole simulated time.

In order to elaborate the global effect of using a detailed cooling function together with a chemical network rather than a simple, parameterized cooling function, we calculated the time evolution of the cold mass fractions and the VFFs for *EI* and *KI* and included them in Figure 5 (turquoise and magenta lines). We find that run *EI* is very similar to *Z0* throughout the driven phase, although cooling seems to be slightly stronger in case of *Z0*, as the VFF of the cold component is somewhat higher with respect to *EI*. On the other hand, in the decaying phase, this effect is reversed after $t = 70$ Myr, where $v_{\text{rms}} \approx 13 \text{kms}^{-1}$. The reduced cooling occurring in run *Z0* with full chemistry is also visible in the cold gas fraction, which drops below *EI* after $t = 70$ Myr.

In summary, we cannot see strong immediate effects of the non-equilibrium chemistry. We note that this finding might have to be revised once the formation of molecules (e.g., H_2) is considered (Gnedin & Kravtsov 2011). Furthermore, our simulations show that using a detailed, time-dependent cooling prescription is still superior to using a parameterized cooling function as the results are much more accurate. Run *KI* continuously overpredicts the fraction of cold gas (by up to 200%) and the VFF of the cold gas.
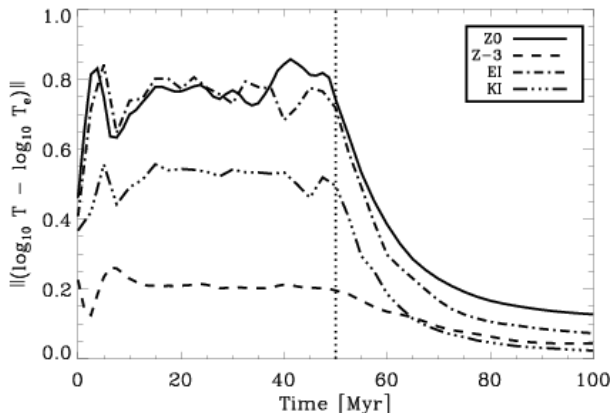
Fig. 6.— Mean deviation of actual gas temperature and equilibrium temperature as a function of time, again for *Z0* (solid line) and *Z-3* (dashed line). In addition, we show run *EI* (dash-dotted line) and run *KI* (dash-dot-dot-dotted line).

4.3. Other effects that may influence the phase distribution

As the variance of the density PDF has been shown to be directly related to the turbulent Mach number (Padoan et al. 1997; Padoan & Nordlund 2002; Federrath et al. 2008), the spread in ρ about the given equilibrium configuration is expected to increase with increasing Mach number M. More compressive driving would enhance this effect (Federrath et al. 2010). Very strong turbulent driving could therefore result in the formation of a stable cold phase even if the metallicity were low. Also our models do not include the effects of self-gravity. Self-gravity is known to cause a power-law tail toward high densities in the den-

sity PDF (Scalo et al. 1998; Klessen et al. 2000; Wada & Norman 2001; Li et al. 2003; Slyz et al. 2005; Kritsuk et al. 2011; Cho & Kim 2011) and therefore would certainly influence the gas density distribution at high ρ. As the powerlaw tail is typically flatter than the log-normal distribution (with power spectral indices of around -1.5) more dense gas would be available for cooling, and the cold component would become more massive leading to more star formation. Therefore, the effect of self-gravity might shift the critical values of turbulent Mach number above which the formation of cold gas is suppressed, and the critical values of metallicity below which the formation of cold gas is suppressed.

The assumed FUV heating rate, Γ_{FUV}, also influences the distribution of phases. In our present study, we assume that the photoelectric heating rate per unit dust mass is the same in both simulations, so that the only change in Γ_{FUV} between the two simulations comes from the change in the total dust mass, which we assume to scale linearly with metallicity. In reality, the composition and size distribution of dust grains in very low metallicity gas may be quite different from what we are used to in the Milky Way, which would lead to an additional change in Γ_{FUV}. The strength of the FUV radiation field is also an influential uncertainty. Decreasing the FUV intensity by a factor of 100 results in a decrease in ρ_{thres} of about a factor of 10 (Wolfire et al. 2003), thus facilitating the formation of a cold component in regions of low star formation. In an upcoming paper we will further discuss the relationship between ρ_{thres}, Z, and Γ_{FUV}, as well as that between VFF and M.

Placed in an astrophysical context, our finding implies that star formation would effectively be inhibited in a system of low metallicity if no event capable of driving strong turbulence (e.g., spiral shocks in a disk galaxy, a merger, or the infall of gas onto a galactic disk) occurred.

5. Conclusions and Astrophysical Context

The dependence of the cooling rate on the metal abundance in the gas shifts the pressure range that allows for the formation of a bi-stable medium toward higher values with decreasing metallicity. Even in the Milky Way, this effect is so influential

that the formation of cold molecular gas is prevented at distances larger than 18 kpc from the Galactic Center where $Z \approx 0.2 \ Z_\odot$ (see analytical estimates by Wolfire et al. 2003; Elmegreen & Elmegreen 1984).

In order to understand this process in greater detail, we have simulated the turbulent evolution of a multi-phase ISM under driven and decaying turbulent conditions at different metallicities ($Z = Z_\odot$ and $Z = 10^{-3}Z_\odot$). This mimics interstellar conditions for different galactic environments. For driven turbulent conditions, we find that metallicity does not have a strong influence on either the shape of the resulting, single-peaked density PDF, or the temperature PDF. However, for $Z = 10^{-3}Z_\odot$ the VFF of the cold component is lower by an approximately constant factor of 20.

In decaying turbulent conditions, we find a clear relation between the abundance of cold gas and the metallicity. Whereas the coldest regions are quickly dispersed in case of low metallicity and the system evolves toward a single component, warm medium, a stable cold component is formed in case of solar metallicity and a double-peaked density PDF is developed. Thus, on a dynamical time scale, the survival of cold clumps is strongly influenced by the gas chemistry. In agreement with previous models of other authors (e.g., Schaye 2004), our numerical simulations imply that the turbulent evolution of the ISM at different metallicities causes systematic changes in the initial conditions for star formation and should strongly affect the global star formation efficiency of a galaxy.

We also find the non-equilibrium chemistry to not have a significant influence on our results at high turbulent velocity dispersions for both, low and solar metallicity. However, in mildly turbulent conditions ($v_{\mathrm{rms}} \overset{<}{\sim} 13 \ \mathrm{km \ s^{-1}}$), the effect of non-equilibrium chemistry becomes more pronounced. Moreover, we find that using an accurate cooling prescription, like the one presented in Glover & Mac Low (2007), rather than a parameterized cooling function is especially important to precisely predict the mass and VFF of the cold gas component in a multi-phase model.

Placed in a more global astrophysical context these results could be meaningful to several fields. We can speculate on the following.

- Metal-poor dwarf galaxies have very low star formation rates (Boissier et al. 2003), which can currently not be reproduced in simulations of dwarf galaxy formation and evolution (Guo et al. 2011; Gnedin & Kravtsov 2010). If an external trigger (e.g., a merger or tidal perturbation) were missing, our chemo-dynamical ISM model would lead to such a low star formation rate.

- Dwarf galaxies seem to have complex star formation histories (e.g., as observed for the Carina dSph by Tolstoy 2003; Burkert & Ruiz-Lapuente 1997). In our model, metal-poor dwarfs could only form stars if the gas were stirred. Hence, clumpy gas infall, tidal effects, or other forms of irregular stirring (e.g., due to gravitational instabilities) would naturally lead to very complex star formation histories in these systems.

- Metal-poor galaxies which have a low star formation rate should be able to slowly accrete a lot of gas – e.g., via gas infall in cold streams (Kereš et al. 2005; Dekel et al. 2009) – without experiencing a significant increase in their star formation rate. Therefore, they would acquire the potential to become progenitors for massive starburst galaxies.

- The star formation rate in merging galaxies is probably not strongly dependent on the gas metallicity if supersonic gas turbulence is driven due to the merger.

REFERENCES

Audit, E. & Hennebelle, P. 2005, A&A, 433, 1

—. 2010, A&A, 511, A76+

Aumer, M., Burkert, A., Johansson, P. H., & Genzel, R. 2010, ApJ, 719, 1230

Banerjee, R., Vázquez-Semadeni, E., Hennebelle, P., & Klessen, R. S. 2009, MNRAS, 398, 1082

Beresnyak, A. & Lazarian, A. 2009, ApJ, 702, 1190

Bigiel, F., Leroy, A., Walter, F., Brinks, E., de Blok, W. J. G., Madore, B., & Thornley, M. D. 2008, AJ, 136, 2846

Boissier, S., Prantzos, N., Boselli, A., & Gavazzi, G. 2003, MNRAS, 346, 1215

Brandenburg, A., Korpi, M. J., & Mee, A. J. 2007, ApJ, 654, 945

Brown, P. N., Byrne, G. D., & Hindmarsh, A. C. 1989, SIAM J. Sci. Stat. Comput., 10, 1038ff

Burkert, A. & Lin, D. N. C. 2000, ApJ, 537, 270

Burkert, A. & Ruiz-Lapuente, P. 1997, ApJ, 480, 297

Cho, W. & Kim, J. 2011, MNRAS, 410, L8

Colella, P. & Woodward, P. 1984, JCP, 54, 174ff

de Avillez, M. A. & Breitschwerdt, D. 2007, ApJ, 665, L35

—. 2010, ArXiv e-prints

Dekel, A., Birnboim, Y., Engel, G., Freundlich, J., Goerdt, T., Mumcuoglu, M., Neistein, E., Pichon, C., Teyssier, R., & Zinger, E. 2009, Nature, 457, 451

Draine, B. T. 1978, ApJS, 36, 595

Elmegreen, B. G. 2002, ApJ, 577, 206

Elmegreen, B. G. & Burkert, A. 2010, ApJ, 712, 294

Elmegreen, D. M. & Elmegreen, B. G. 1984, ApJS, 54, 127

Federrath, C., Klessen, R. S., & Schmidt, W. 2008, ApJ, 688, L79

Federrath, C., Roman-Duval, J., Klessen, R. S., Schmidt, W., & Mac Low, M. 2010, A&A, 512, A81+

Field, G. B. 1965, ApJ, 142, 531

Fryxell, B., Olson, K., Ricker, P., Timmes, F. X., Zingale, M., Lamb, D. Q., MacNeice, P., Rosner, R., Truran, J. W., & Tufo, H. 2000, ApJS, 131, 273

Genzel, R., Tacconi, L. J., Eisenhauer, F., Förster Schreiber, N. M., Cimatti, A., Daddi, E., Bouché, N., Davies, R., Lehnert, M. D., Lutz, D., Nesvadba, N., Verma, A., Abuter, R., Shapiro, K., Sternberg, A., Renzini, A., Kong, X., Arimoto, N., & Mignoli, M. 2006, Nature, 442, 786

Glover, S. C. O. 2003, ApJ, 584, 331

Glover, S. C. O., Federrath, C., Mac Low, M., & Klessen, R. S. 2010, MNRAS, 404, 2

Glover, S. C. O. & Mac Low, M. 2007, ApJ, 659, 1317

—. 2011, MNRAS, 412, 337

Gnedin, N. Y. & Kravtsov, A. V. 2010, ApJ, 714, 287

—. 2011, ApJ, 728, 88

Gnedin, N. Y., Tassis, K., & Kravtsov, A. V. 2009, ApJ, 697, 55

Guo, Q., White, S., Boylan-Kolchin, M., De Lucia, G., Kauffmann, G., Lemson, G., Li, C., Springel, V., & Weinmann, S. 2011, MNRAS, 164

Heitsch, F., Hartmann, L. W., Slyz, A. D., Devriendt, J. E. G., & Burkert, A. 2008, ApJ, 674, 316

Heitsch, F., Slyz, A. D., Devriendt, J. E. G., Hartmann, L. W., & Burkert, A. 2006, ApJ, 648, 1052

Hennebelle, P., Banerjee, R., Vázquez-Semadeni, E., Klessen, R. S., & Audit, E. 2008, A&A, 486, L43

Hennebelle, P. & Chabrier, G. 2008, ApJ, 684, 395

Hussaini, M. Y., van Leer, B., & Rosendale, J. V., eds. 1997, Upwind and High-Resolution Schemes (Berlin: Springer)

Joung, M. K. R. & Mac Low, M. 2006, ApJ, 653, 1266

Kanekar, N., Subrahmanyan, R., Chengalur, J. N., & Safouris, V. 2003, MNRAS, 346, L57

Karl, S. J., Naab, T., Johansson, P. H., Kotarba, H., Boily, C. M., Renaud, F., & Theis, C. 2010, ApJ, 715, L88

Kennicutt, Jr., R. C., Calzetti, D., Walter, F., Helou, G., Hollenbach, D. J., Armus, L., Bendo, G., Dale, D. A., Draine, B. T., Engelbracht, C. W., Gordon, K. D., Prescott, M. K. M., Regan, M. W., Thornley, M. D., Bot, C., Brinks, E., de Blok, E., de Mello, D., Meyer, M., Moustakas, J., Murphy, E. J., Sheth, K., & Smith, J. D. T. 2007, ApJ, 671, 333

Kereš, D., Katz, N., Weinberg, D. H., & Davé, R. 2005, MNRAS, 363, 2

Kitsionas, S., Federrath, C., Klessen, R. S., Schmidt, W., Price, D. J., Dursi, L. J., Gritschneder, M., Walch, S., Piontek, R., Kim, J., Jappsen, A., Ciecielag, P., & Mac Low, M. 2009, A&A, 508, 541

Klessen, R. S., Heitsch, F., & Mac Low, M. 2000, ApJ, 535, 887

Koyama, H. & Inutsuka, S. 2000, ApJ, 532, 980

—. 2002, ApJ, 564, L97

Kritsuk, A. G. & Norman, M. L. 2002, ApJ, 569, L127

—. 2004, ApJ, 601, L55

Kritsuk, A. G., Norman, M. L., Padoan, P., & Wagner, R. 2007, ApJ, 665, 416

Kritsuk, A. G., Norman, M. L., & Wagner, R. 2011, ApJ, 727, L20+

Krumholz, M. R., Leroy, A. K., & McKee, C. F. 2011, ApJ, 731, 25

Krumholz, M. R. & McKee, C. F. 2005, ApJ, 630, 250

Krumholz, M. R., McKee, C. F., & Tumlinson, J. 2009, ApJ, 699, 850

Leroy, A. K., Walter, F., Brinks, E., Bigiel, F., de Blok, W. J. G., Madore, B., & Thornley, M. D. 2008, AJ, 136, 2782

Li, Y., Klessen, R. S., & Mac Low, M. 2003, ApJ, 592, 975

Mac Low, M. 1999, ApJ, 524, 169

McKee, C. F. & Ostriker, J. P. 1977, ApJ, 218, 148

Motte, F., Andre, P., & Neri, R. 1998, A&A, 336, 150

Nutter, D. & Ward-Thompson, D. 2007, MNRAS, 374, 1413

Omukai, K., Tsuribe, T., Schneider, R., & Ferrara, A. 2005, ApJ, 626, 627

Ostriker, E. C., McKee, C. F., & Leroy, A. K. 2010, ApJ, 721, 975

Ostriker, E. C., Stone, J. M., & Gammie, C. F. 2001, ApJ, 546, 980

Padoan, P., Jones, B. J. T., & Nordlund, A. P. 1997, ApJ, 474, 730

Padoan, P. & Nordlund, Å. 2002, ApJ, 576, 870

—. 2011, ApJ, 730, 40

Pavlovski, G., Smith, M. D., Mac Low, M., & Rosen, A. 2002, MNRAS, 337, 477

Pelupessy, F. I. & Papadopoulos, P. P. 2009, ApJ, 707, 954

Pikel'Ner, S. B. 1968, ARA&A, 6, 165

Price, D. J., Federrath, C., & Brunt, C. M. 2011, ApJ, 727, L21+

Robertson, B. E. & Kravtsov, A. V. 2008, ApJ, 680, 1083

Scalo, J., Vazquez-Semadeni, E., Chappell, D., & Passot, T. 1998, ApJ, 504, 835

Schaye, J. 2004, ApJ, 609, 667

Schaye, J. & Dalla Vecchia, C. 2008, MNRAS, 383, 1210

Slyz, A. D., Devriendt, J. E. G., Bryan, G., & Silk, J. 2005, MNRAS, 356, 737

Spaans, M. & Carollo, C. M. 1997, ApJ, 482, L93+

Spaans, M. & Norman, C. A. 1997, ApJ, 483, 87

Tasker, E. J. & Bryan, G. L. 2008, ApJ, 673, 810

Teyssier, R., Chapon, D., & Bournaud, F. 2010, ApJ, 720, L149

Tolstoy, E. 2003, Ap&SS, 284, 579

Vazquez-Semadeni, E. 2009, ArXiv e-prints

Vázquez-Semadeni, E., Gómez, G. C., Jappsen, A. K., Ballesteros-Paredes, J., González, R. F., & Klessen, R. S. 2007, ApJ, 657, 870

Wada, K. & Norman, C. A. 2001, ApJ, 547, 172

—. 2007, ApJ, 660, 276

Wolfire, M. G., Hollenbach, D., McKee, C. F., Tielens, A. G. G. M., & Bakes, E. L. O. 1995, ApJ, 443, 152

Wolfire, M. G., McKee, C. F., Hollenbach, D., & Tielens, A. G. G. M. 2003, ApJ, 587, 278

Wong, T. & Blitz, L. 2002, ApJ, 569, 157

Woodward, P. & Colella, P. 1984, JCP, 54, 115ff